ACS APPLIED MATERIALS & INTERFACES

Research Article

www.acsami.org

Core–Shell Sn–Ni–Cu-Alloy@Carbon Nanorods to Array as Three-Dimensional Anode by Nanoelectrodeposition for High-Performance Lithium Ion Batteries

Hao Peng, Rui Li,* Jiangtao Hu, Wenjun Deng, and Feng Pan*

School of Advanced Materials, Peking University, Peking University Shenzhen Graduate School, Shenzhen 518055, China

Supporting Information

ABSTRACT: We report the synthesis of a novel three-dimensional anode based on the core–shell Sn–Ni–Cu-alloy@carbon nanorods which was fabricated by pulse nanoelectrodeposition. Li ion batteries equipped with the three-dimensional anode demonstrated almost 100% capacity retention over 400 cycles at 450 mA g^{-1} and excellent rate performance even up to 9000 mA g^{-1} for advanced Li-ion battery. Insight of the high performance can be attributed to three key factors, Li–Sn alloys for Li-ion storage, Ni–Cu matrix for the electronic conductive and nanorods structure, and the carbon shell for the electronic/Li-ion conductive and holding stable solid electrolyte interphase (SEI), because these shells always kept stable volumes after extension of initial charge–discharge cycles.

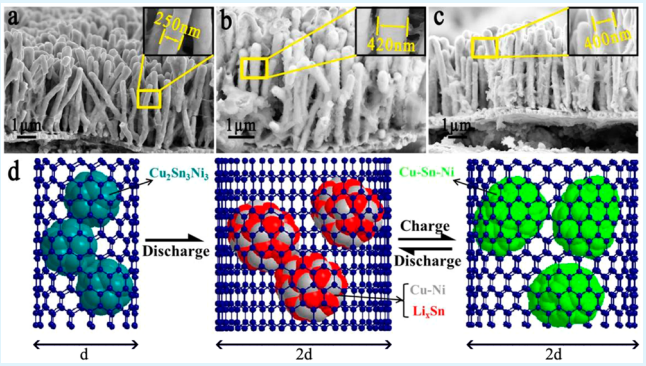

KEYWORDS: *core–shell, alloy, carbon coating, nanorods, three-dimensional, Lithium-ion battery*

1. INTRODUCTION

Lithium ion batteries (LIBs) have attracted great attention around the world. Every year, countless LIBs are applied to electric vehicles and portable electronic devices.[1] Due to their high theoretical capacity (992 mAh g^{-1}) and the abundance of tin in nature, tin-based anode materials have been widely projected as one of the most promising candidate in substitute of the already commercialized graphite (372 mAh g^{-1}). In 1995, Fuji Photo Film Corporation proposed amorphous Sn-based composite for lithium-ion battery anode with good cycling performance.[2] This work was later reported in *Science* in 1997 and attracted widespread attention.[3] However, problems still exist in Sn-based anodes like the large volume expansion (~300%) during charge/discharge processes, which can make the anode materials easily pulverized and cracked to raise really a big problem to keep good cycling performance and high rate performance for practical application.[4] To alleviate the problems, a series of Sn-based intermetallic alloys have been investigated, such as Sn–Ni,[5] Sn–Sb,[6] Sn–Co,[7] Sn–Cu,[8] Sn–Fe,[9] Sn–Al,[10] and Sn–C,[11] alloy. In 1996, Yang et al. prepared nanosized Sn and SnSb, SnAg intermetallic alloys by electrodeposition, and the cycling performance was obviously improved.[12,13] Later, Mukaibo et al. prepared Sn–Ni alloy by electrodeposition and found that the material with 62% tin atoms showed the best cycling performance.[14] In 2005, Sony Corporation achieved industrialization of SnCoC alloy anode material for its high specific capacity as the first time alloy anode material was applied in industrial production.[15] In 2006, Dahn et al. synthesized several kinds of Sn–M–C (M = Ti/V/Co) ternary material by magnetron sputtering and found the reason why SnCoC performed the best.[16,17] In 2011, Wang et al. used phenol formaldehyde resin as the carbon source and $SnCl_4$ as the tin source to prepare a Sn–C nanocomposite material. This material could exhibit an excellent cyclability like 588 mAh g^{-1} and 36 mAh g^{-1} at the current density of 20 mA g^{-1} and 200 mA g^{-1}.[18]

Recently, a lot of work has been done to study the core–shell structure for Li-ion battery to take advantages of the cores for Li-ion storage and shell for the generation of stable SEI.[19−21] In 2012, Cui's group designed a double-wall core–shell structure with Si nanoparticles at the core for storing Li-ions, and SiO_2 as a hard shell for protecting the volume change during charge–discharge and for forming stable SEI films. This type of structure greatly improved the electrochemical performance of Si anode.[22,23] In 2015, Hu et al. developed a core–shell Fe_2O_3@graphene anode, in which the γ-Fe_2O_3 core is for Li-ion storage and the graphene shell is for both creating stable SEI films and enhancing the electron/Li-ion conductivity. As a result, enhanced long-term charge–discharge cycling stability and charging rate were achieved.[24]

Here, we successfully developed core–shell Sn–Ni–Cu-alloy@carbon nanorods to array as three-dimensional anode by

Received: March 19, 2016
Accepted: April 26, 2016

DOI: 10.1021/acsami.6b03383
ACS Appl. Mater. Interfaces XXXX, XXX, XXX–XXX

pulse nanoelectrodeposition and thermal treating. In Sn−Ni−Cu-alloy cores, Li−Sn alloys play a role for Li-ion storage, and Ni−Cu alloy is a Li-inactive element and works as a buffer matrix, which can maintain the entire structure as a stable framework and also support the electronic conduction.[5,25,26] The carbon shells, which were generated by the nickel as a catalyst to catalysis better graphitized carbon during decomposition of the coating polycarbonate membrane on the surface of the Sn−Ni−Cu nanorods calcined at 550 °C in argon and hydrogen gas mixture, can support for the electronic/Li-ion conductive and holding stable SEI by protection of volumes variations during lithiation/delithiation of Sn−Ni−Cu alloys.

2. MATERIALS AND METHODS

The tin−nickel alloy nanorods were prepared by electrodeposition inside the nanoscale pores of track-etched polycarbonate membranes (Whatman Nuclepore, with nominal pore diameter of 200 nm). The formation process is showed as Scheme 1.

Scheme 1. Schematic Illustration of the Preparation of the Core−Shell Sn−Ni−Cu−Alloy@Carbon Nanorods Array

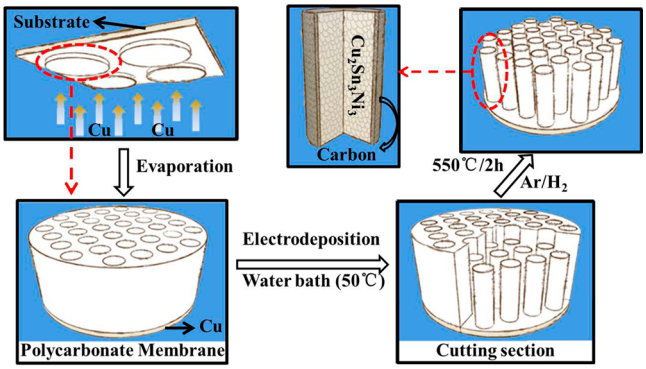

First of all, a copper film was evaporated on one side of the membrane to create a conductive surface then to be glued by a conductive paste to a copper foil as the current collector. Subsequently, the Sn−Ni alloy nanorods were nanoelectrodeposited into the nanoscale pores of track-etched polycarbonate membranes. The Sn−Ni alloy nanorods electrodeposition conditions were monitored by using a Maccor Series MC-16 battery testing system. An aqueous solution, formed by $SnSO_4$ 0.175 M, $NiSO_4$ 0.075 M, $K_4P_2O_7$ 0.5 M, glycine 0.125 M and NH_4OH 5 mL L^{-1}, was used with a graphite plate as the counter electrode.[14] The electrodeposition was conducted under pulsed current of approximately 7 mA cm^{-2} for 2000s, whose frequency is 1 Hz with an on/off ratio waveform of 1:9. The working temperature was maintained by a water bath at 50 °C. The electrodeposited product was washed with deionized water and was dried at 80 °C under air atmosphere. Hereafter, the dry obtained product was calcined at 550 °C in mixture gas of argon and 10% hydrogen for 2 h. During the calcination process, it was found that the copper atoms from the current collector diffused into the Sn−Ni alloy nanorods to produce the Sn−Ni−Cu alloy nanorods, while carbon atoms decomposed from the polycarbonate permeated into the superficial layer of the nanorods to generate NiC_x layer. When cooling to room temperature, the dissolved carbon atoms dissolved out as amorphous carbon and coated the surface of the alloy nanorods.[27] As the furnace cooled naturally to room temperature, a main Sn−Ni−Cu ternary alloy phase formed. (Scheme 1)

3. RESULTS AND DISCUSSION

3.1. Physical Structure and Morphology of the Core−Shell Sn−Ni−Cu-Alloy@Carbon Nanorods Array. The crystalline structure of the prepared core−shell Sn−Ni−Cu-alloy@carbon nanorods array was further characterized by X-ray diffraction (XRD) using Cu Kα radiation (λ = 0.15418 nm) (Figure 1a). It can be proved by XRD, ICP and XPS that the Sn−Ni−Cu-alloy is mainly $Cu_2Ni_3Sn_3$. The diffraction peaks of the alloy nanorods match to that of $Cu_2Ni_3Sn_3$ at 30.26, 34.52, 42.96, 43.59, 53.99, 56.80, 59.26, 62.86, 71.77, 72.84, and 80.03°, corresponding to crystal planes of (101), (002), (102), (110), (201), (112), (103), (202), (211), (004) and (300). Moreover, ICP analysis was conducted to confirm the composition of the Sn−Ni−Cu alloy electrode and the results revealed that the atomic ratio of Sn/Ni was almost 1:1. What's more, in EDS analysis (Figure S1), the distribution of Sn, Ni, and Cu atoms were almost the same. XPS spectra in Figure S2 show the Sn 3d, Ni 2p, and Cu 2p spectra at different state. For Sn, Sn $3d_{5/2}$ at 485.08 eV and Sn $3d_{5/2}$ at 486.5 eV are assigned to metallic tin (Sn (0)) and oxidized tin (Sn (IV)), respectively. As shown in the figure, we can find that the peaks at 485.08 eV become stronger and stronger as the etching time goes from 0s to 90s which indicates that the surface of Sn−Ni−Cu alloy is covered by a thin oxide tin layer resulting from the exposure of samples to atmosphere. And inside the alloy the component of tin is metallic tin (Sn (0)).[28] For Ni, the binding energy of 853.1 eV to Ni $2p_{3/2}$ XPS spectrum is assigned to Ni (0).[29] And for Cu, the binding energy of 933.1 eV to Cu $2p_{3/2}$ XPS spectrum is assigned to Cu (0).[30]

The SEM images in Figure S3 show the morphology of the core−shell Sn−Ni−Cu-alloy@carbon nanorods array. It is obvious that carbon was not only coated on the surface of the nanorods, but also dispersed in the uniform interspacing among the nanorods. The continuous carbon net inevitably contributes to better conductivity and better structure stability. The Raman spectrum of the carbon coating on the alloy nanorods samples in Figure 1c showed that there were two characteristic peaks at 1350 and 1593 cm^{-1}, which corresponded to the D band and G band of carbon (I_G/I_D = 1.16), respectively. The D-band is a sign of the defects and disordered portions of carbon, while G-band illustrates the order graphitic crystallites of carbon. Generally speaking, the higher the ratio of I_G/I_D is, the greater the degree of graphitization.[31] The high-resolution C 1s XPS spectrum of the samples (Figure 1b) can be fitted into four components, corresponding to carbon atoms in four different chemical environments: carbon sp^2 (284.5 eV), carbon sp^3 (285.2 eV), the carbon in C−O (286.2 eV), and the carbonyl carbon (C═O) at 287.9 eV. The percentage of carbon sp^2 is 66.77%, which also demonstrates a high graphitization degree.[32] For better research on the carbon shell, we used hydrochloric acid to dissolve the Sn−Ni−Cu-alloy core, and we successfully obtained the pure carbon shell nanorods (Figure S4). As shown in Figure 1d, the carbon shell could still keep a very stable structure even with the alloy core dissolved. And according to the SAED pattern, we find that the carbon is amorphous carbon. The TEM image in Figure 1e shows the border between the alloy and the carbon. Also we can distinguish several crystal planes of the alloy like (002) and (101) planes with the same interplanar crystal spacing as the XRD data tells. And the thickness of carbon is approximately 4−5 nm uniformly. So, we can believe that much amorphous carbon were formed on the surface of the Sn−Ni−Cu alloy nanorods during the heating and cooling process. The mechanism of generation of the better graphitized carbon shell could be resulted from that when the polycarbonate was decomposed into carbon, the carbon atoms would gradually seep into the nickel surface to form carburizing solid solution (Ni_xC) under a

DOI: 10.1021/acsami.6b03383
ACS Appl. Mater. Interfaces XXXX, XXX, XXX−XXX

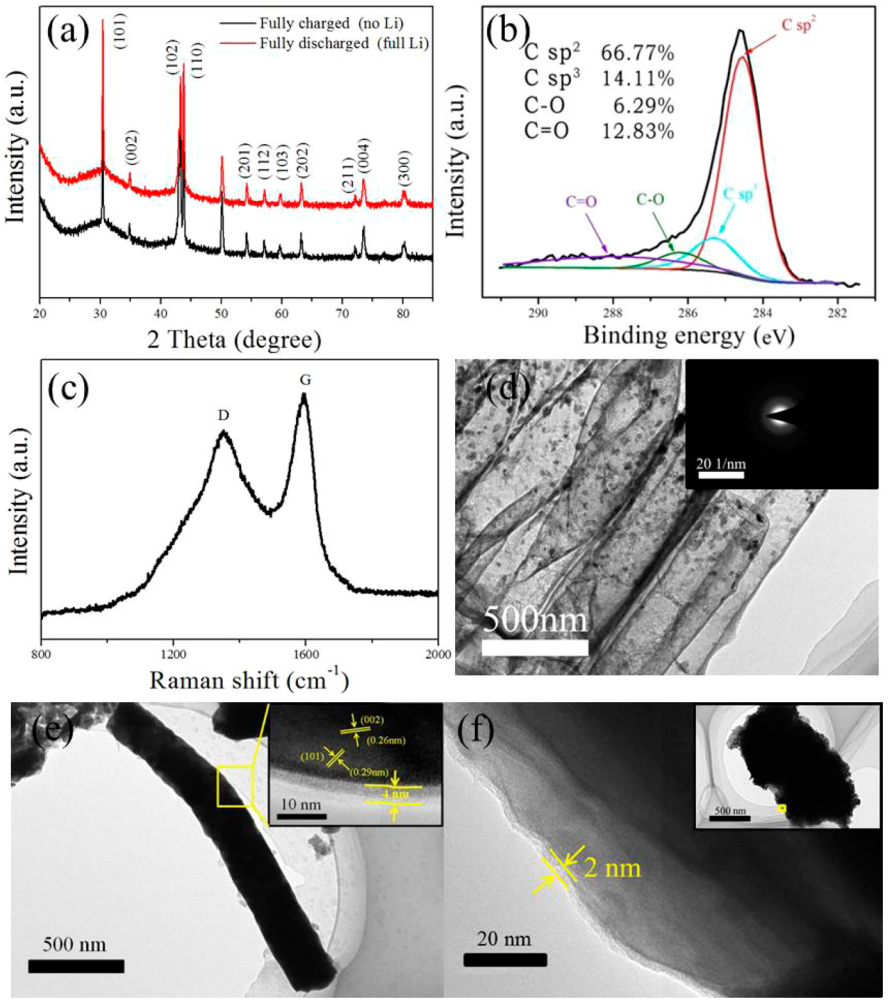

Figure 1. (a) XRD patterns for the samples fully charged and fully discharged; (b) C 1s spectra of the core−shell Sn−Ni−Cu-alloy@carbon nanorods array anode; (c) Raman spectrum of the core−shell Sn−Ni−Cu-alloy@carbon nanorods array anode; (d) TEM image of the carbon shells with an inset showing the SAED pattern; and (e and f) TEM images of the core−shell Sn−Ni−Cu-alloy@carbon nanorods array anode before cycles and after 1000 cycles.

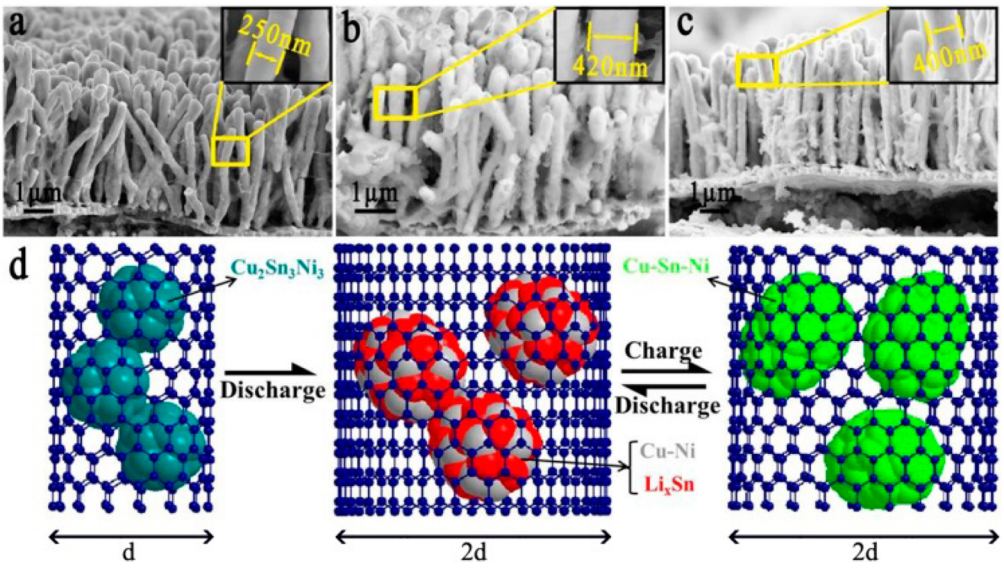

Figure 2. Cross-sectional view of SEM images of the core−shell Sn−Ni−Cu-alloy@carbon nanorods array anode (a) origin state; (b) full of lithium after 10 cycles; (c) empty of lithium after 10 cycles; (d) the schematic illustration of the change of carbon shell and alloy during the charge−discharge process.

DOI: 10.1021/acsami.6b03383
ACS Appl. Mater. Interfaces XXXX, XXX, XXX−XXX

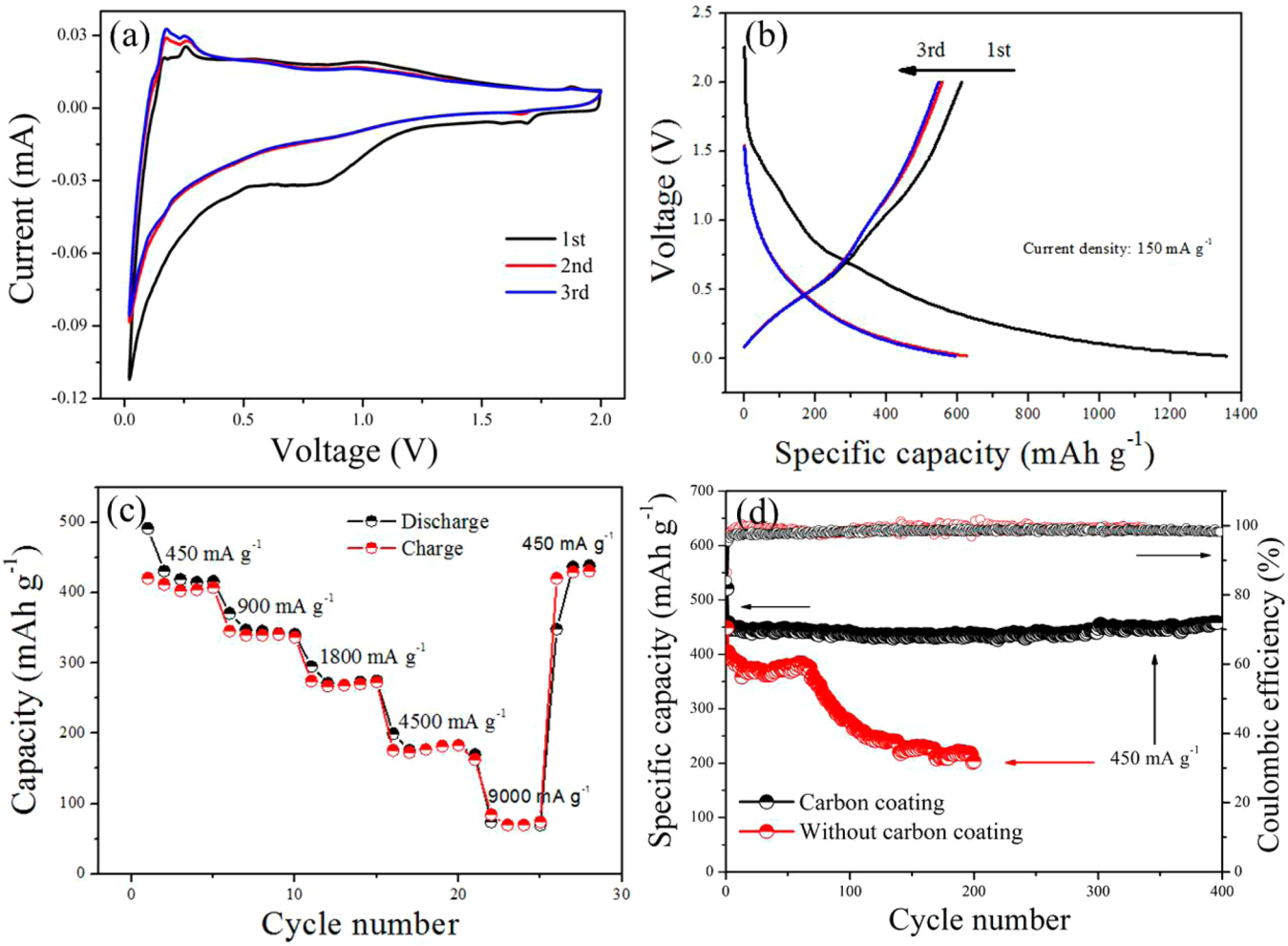

Figure 3. Electrochemical performance for the core−shell Sn−Ni−Cu-alloy@carbon nanorods array anode: (a) the cyclic voltammograms; (b) the charge−discharge curves at 150 mA g^{-1}; (c) rate performances at different current density; (d) cycling performance at 450 mA g^{-1} for different samples with carbon coating and without carbon coating.

high temperature around 550 °C. During the cooling process, carbon atoms would separate out from the carburizing solid solution and form carbon layers on the surface of Sn−Ni−Cu alloy nanorods.[33]

3.2. Physical and Electrochemical Performance of the Core−Shell Sn−Ni−Cu-Alloy@Carbon Nanorods Array Anode. The core−shell nanorods arrayed as three-dimensional anode were used for performance measurement of Li-ion battery. Half cells were assembled with lithium foils as the counter electrodes. The loading mass of the core−shell nanorods array anode was calculated in an indirect way. We used TGA to figure out the carbon content and ICP to confirm the alloy mass, and we added up the two parts to get the final loading mass afterward. The samples were tested in a voltage window of 0.01 to 2 V. The entire structure could be kept integrated during the charging/discharging process, so could the Ni−Cu matrix (Figure 1a). As shown in Figure 2, the original diameter of the core−shell Sn−Ni−Cu-alloy@carbon nanorod was almost 250 nm. When fully lithiated after 10 cycles, the diameter was extended to almost 420 nm, the volume of the nanorods can be expanded two or three times, and the carbon shell will extend meanwhile. When fully delithiated after 10 cycles, the diameter still remained almost 400 nm, which illustrated that the carbon shell kept a stable volume during cycles once fully expanded. Interestingly, according to the TEM images in Figure 1f, the thickness of carbon layer after long cycles decreased to almost two nanometers from four to five nanometers of the original nanorod before cycles, which meant that carbon layers would expand to become thinner during extension to fit the large volume change. Thus, the carbon shell can keep a stable size to provide a conductive network during long cycles, which can predict that without the minimum volume variation the SEI film would always keep stable meanwhile. Furthermore, even after 1000 cycles checked with TEM (similar to Figure 1f), the carbon shell still existed and the SEI film kept stable, which should be able to contribute to a superior electrochemical performance, including excellent cycle stability and rate capability.

The electrochemical performances of the core−shell Sn−Ni−Cu-alloy@carbon nanorods array anode were systematically investigated. The CV curve is showed in Figure 3a. There are two peaks during the charging curve near 0.6 and 1.0 V, which represent the different delithiation process, respectively.[34] As the figures show, the core−shell samples showed an extremely good cycle stability at the current density of 450 mA g^{-1}, which was much better than the samples without carbon coating. Up to 400 cycles, there were almost no degradations (Figure 3d). Even at the current density of 2250 mA g^{-1}, the core−shell samples could still keep high cycle stability, for

DOI: 10.1021/acsami.6b03383
ACS Appl. Mater. Interfaces XXXX, XXX, XXX−XXX

example, by which 70% of capacity will remain up to more than 600 cycles (Figure S5). Also an outstanding rate performance of the core−shell sample has been observed with various current densities from 450 mA g^{-1} to 9000 mA g^{-1}. The core−shell electrode could deliver stable capacities under different current rate, and the capacity could recover to its initial value when the current rate was turned back to 450 mA g^{-1} after a very high current rate (9000 mA g^{-1}) with different cycling schedules (Figure 3c). The electrochemical performance of our core−shell materials is better than those of the Sn-based anode reported in literatures. (Table 1)

Table 1. Comparison of Sn-based Materials for Lithium Ion Batteries

material	cycling performance	morphology	ref
Sn−Ni	0.8C/500 mAh g^{-1} for 200 cycles	nanorod	5
Sn−C	0.1C/450 mAh g^{-1} for 100 cycles	core−shell	35
Sn−C	0.25C/710 mAh g^{-1} for 130 cycles	sphere	36
Sn−C	3000 mA g^{-1}/537 mAh g^{-1} for 1000 cycles	nanocube	11
Sn-CNT	0.5C/380.9 mAh g^{-1} for 1000 cycles	nanotube array	37

3.3. Mechanism Analysis. Note that the carbon coating on the surface of the alloy nanorods has significantly influenced the performance of charging/discharging rates and cycle stability. One key function of the carbon shell is to form a conductive network that can facilitate electron transport and improve the electronic conductivity. This was also validated by our electrochemical impedance spectroscopy (EIS) measurements (Figure 4a,b). Electrochemical impedance spectroscopy (EIS) studies were carried out after 1, 2, 5, and 10 cycles at 450 mA g^{-1} for both samples with and without carbon coating, and the frequency range was from 10 mHz to 100 kHz. For the core−shell Sn−Ni−Cu-alloy@carbon nanorods array anode, all the different frequency parts showed better stability than the samples without carbon coating. We could find that the samples with carbon coating had lower bulk impendence and higher diffusion coefficient than the samples without carbon coating. In a word, the SEI film of the core−shell Sn−Ni−Cu−alloy@carbon nanorods array anode was more stable, and also had better electrochemical performance. So another key function of the carbon shell is to generate a stable structure which could protect the nanorods from pulverization and provide a stable SEI film during lithiation/delithiation cycles. The SEM images in Figure 4c,d and Figure S6 showed the two different nanarod array anodes with and without carbon coating after 200 cycles. Apparently, the sample with carbon coating had an obvious protective layer on the surface, and the alloy core was protected very well, but the sample without carbon coating showed a very rough interface and obvious no stable protective layer. The element mapping of the core−shell Sn−Ni−Cu-alloy@carbon nanorod after 200 cycles in Figure S7 showed clear signal of fluorine and oxygen, which to some extent indicated the SEI formation on the surface.[38] Figure 2d shows the schematic illustration of the change of carbon shell and alloy during the

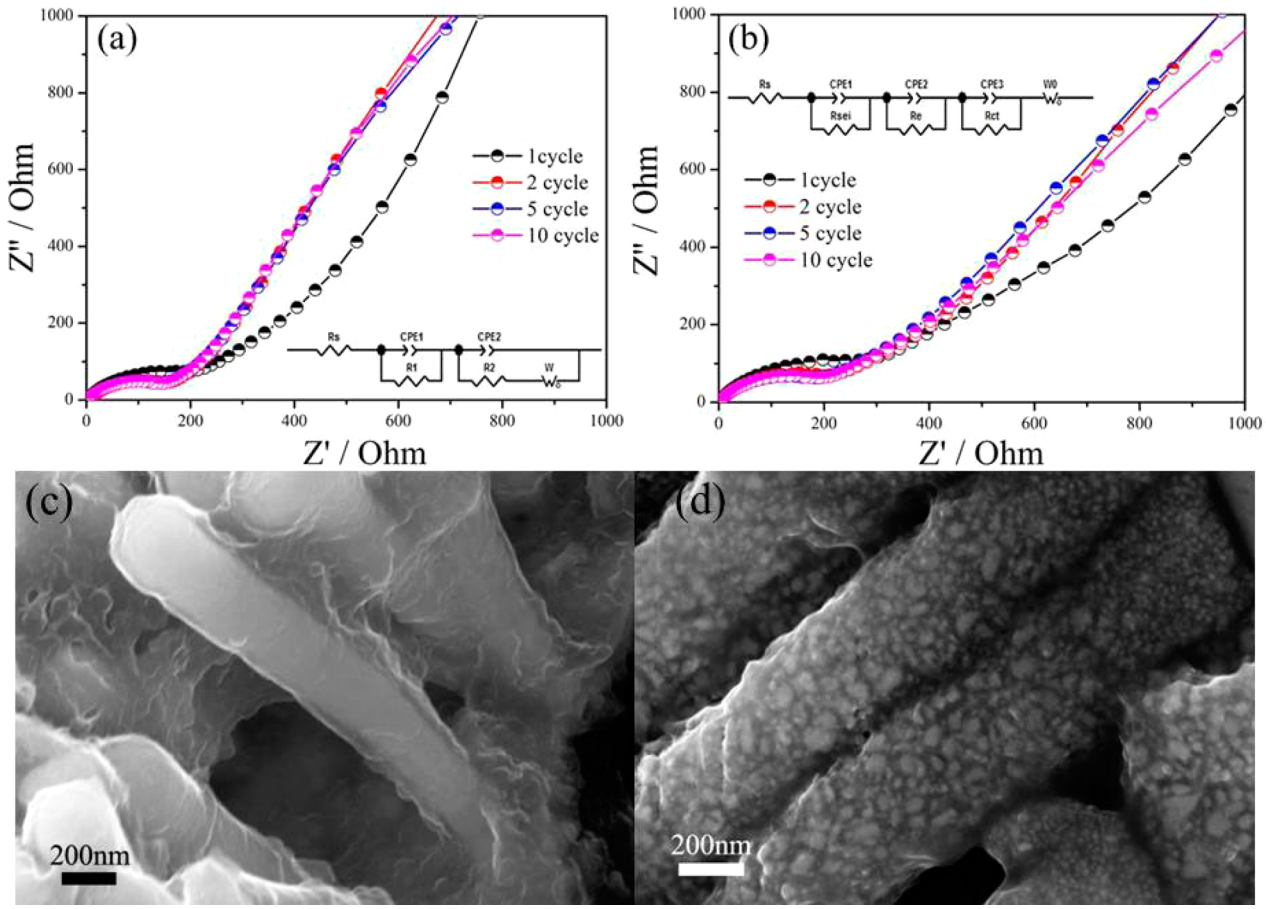

Figure 4. (a and b) EIS data and equivalent circuits of the samples with and without carbon coating; (c and d) SEM images of the samples with and without carbon coating after 200 cycles.

DOI: 10.1021/acsami.6b03383
ACS Appl. Mater. Interfaces XXXX, XXX, XXX−XXX

charge−discharge process. During the initial and later charging (lithiation), the $Cu_2Sn_3Ni_3$ alloy will change as the Li-ion active Li_xSn (x = 0−4.4) alloy and Li-ion inactive Cu−Ni alloy matrix in the nanorod. After the initial and later full-discharging (delithiation), the Sn−Cu−Ni alloy is generated, in which Sn nanoparticles may be loaded on Cu−Ni matrix. Note that Figure 1a shows that the XRD are almost the same during lithiation/delithiation cycles, which can support that the Cu−Ni alloy could consistently maintain a stable matrix. However, Cu−Ni alloy and $Cu_2Ni_3Sn_3$ have some peaks overlapped at 43.60, 50.79, and 74.68°, which may lead to that XRD shows no significant change in lithiation and delithiation. Thus, the special nanorods structure played an important role for the high performance Li-ion battery, in which the Cu−Ni matrix structure could not only provide a structural buffering framework to cushion the mechanical stress caused by the large volume change during the charge/discharge process, but also supply framework to contact and link to the carbon shell to improve the electronic conductivity and Li-ion conductivity, which results in shortening the Li-ion diffusion distance to ensure good lithium permeability.

4. CONCLUSIONS

A significant electrochemical performance improvement was achieved by constructing the core−shell Sn−Ni−Cu−alloy@carbon nanorods by nanoelectrodeposition to array as three-dimensional electrodes. The new architecture offered interspace for the large volume change and excellent electronic/Li-ionic conductivity due to the stable carbon shell and Cu−Ni alloy framework. Hence, the three-dimensional core−shell nanorods array anodes exhibit outstanding capacity retention with a high charge/discharge rate, whose performances are much better than those reported in literatures. Such novel core−shell Sn-alloy nanostructures and fundamental understanding of Li-ion storage and effective migration would enable to help design advanced Sn-based anode materials with better stability.

■ ASSOCIATED CONTENT

Supporting Information

The Supporting Information is available free of charge on the ACS Publications website at DOI: 10.1021/acsami.6b03383.

Detailed description of the experiments. Additional figures about EDS/XPS/SEM characterization and electrochemical performance. Additional table about the performance comparison with other Sn-based materials. (PDF)

■ AUTHOR INFORMATION

Corresponding Authors

*Tel: 86-755-26033200. E-mail: panfeng@pkusz.edu.cn.
*E-mail: lirui@pkusz.edu.cn.

Notes

The authors declare no competing financial interest.

■ ACKNOWLEDGMENTS

This research was supported by Guangdong Innovation Team Project (No. 2013N080), ShenZhen Peacock Plan (Grant No. KYPT20141016105435850), Shenzhen Science and Technology Innovation Committee Grant (No. JCYJ20130329175646121, and JCYJ20140509093817681).

■ REFERENCES

(1) Yoshino, A. The Birth of the Lithium-Ion Battery. *Angew. Chem., Int. Ed.* **2012**, *51* (24), 5798−5800.
(2) Idota, Y., *Nonaqueous Secondary Battery*, 1995 US5478671 A.
(3) Idota, Y. Tin-Based Amorphous Oxide: A High-Capacity Lithium-Ion-Storage Material. *Science* **1997**, *276* (5317), 1395−1397.
(4) Winter, M.; Besenhard, J. O. Electrochemical Lithiation of Tin and Tin-based Intermetallics and Composites. *Electrochim. Acta* **1999**, *45* (1−2), 31−50.
(5) Hassoun, J.; Panero, S.; Simon, P.; Taberna, P. L.; Scrosati, B. High-Rate, Long-Life Ni−Sn Nanostructured Electrodes for Lithium-Ion Batteries. *Adv. Mater.* **2007**, *19* (12), 1632−1635.
(6) Wachtler, M.; Winter, M.; Besenhard, J. O. Anodic Materials for Rechargeable Li-batteries. *J. Power Sources* **2002**, *105* (2), 151−160.
(7) Ferrara, G.; Arbizzani, C.; Damen, L.; Guidotti, M.; Lazzari, M.; Vergottini, F. G.; Inguanta, R.; Piazza, S.; Sunseri, C.; Mastragostino, M. High-performing Sn−Co Nanowire Electrodes as Anodes for Lithium-ion Batteries. *J. Power Sources* **2012**, *211*, 103−107.
(8) Pu, W.; He, X.; Ren, J.; Wan, C.; Jiang, C. Electrodeposition of Sn−Cu Alloy Anodes for Lithium Batteries. *Electrochim. Acta* **2005**, *50* (20), 4140−4145.
(9) Yoon, S.; Lee, J.-M.; Kim, H.; Im, D.; Doo, S.-G.; Sohn, H.-J. An Sn−Fe/Carbon Nanocomposite as an Alternative Anode Material for Rechargeable Lithium Batteries. *Electrochim. Acta* **2009**, *54* (10), 2699−2705.
(10) Hu, R.; Shi, Q.; Wang, H.; Zeng, M.; Zhu, M. Influences of Composition on the Electrochemical Performance in Immiscible Sn-Al Thin Films as Anodes for Lithium Ion Batteries. *J. Phys. Chem. C* **2009**, *113* (43), 18953−18961.
(11) Huang, X.; Cui, S.; Chang, J.; Hallac, P. B.; Fell, C. R.; Luo, Y.; Metz, B.; Jiang, J.; Hurley, P. T.; Chen, J. A Hierarchical Tin/Carbon Composite as an Anode for Lithium-ion Batteries with a Long Cycle Life. *Angew. Chem., Int. Ed.* **2015**, *54* (5), 1490−1493.
(12) Yang, J.; Winter, M.; Besenhard, J. O. Small Particle Size Multiphase Li-alloy Anodes for Lithium-ion-batteries. *Solid State Ionics* **1996**, *90* (1−4), 281−287.
(13) Besenhard, J. O.; Yang, J.; Winter, M. Will Advanced Lithium-alloy Anodes Have a Chance in Lithium-ion Batteries? *J. Power Sources* **1997**, *68* (1), 87−90.
(14) Mukaibo, H.; Sumi, T.; Yokoshima, T.; Momma, T.; Osaka, T. Electrodeposited Sn-Ni Alloy Film as a High Capacity Anode Material for Lithium-Ion Secondary Batteries. *Electrochem. Solid-State Lett.* **2003**, *6* (10), A218−A220.
(15) Morrison, D. New Materials Extend Li-ion Performance. *Power Electron. Technol.* **2006**, *32* (1), 50−52.
(16) Dahn, J. R.; Mar, R. E.; Abouzeid, A. Combinatorial Study of $Sn_{1-x}Co_x$ ($0 < x < 0.6$) and $[Sn_{0.55}Co_{0.45}]_{1-y}C_y$ ($0 < y < 0.5$) Alloy Negative Electrode Materials for Li-Ion Batteries. *J. Electrochem. Soc.* **2006**, *153* (2), A361−A365.
(17) Ferguson, P. P.; Martine, M. L.; Dunlap, R. A.; Dahn, J. R. Structural and Electrochemical Studies of $(Sn_xCo_{1-x})_{60}C_{40}$ Alloys Prepared by Mechanical Attriting. *Electrochim. Acta* **2009**, *54* (19), 4534−4539.
(18) Wang, J.; Li, D.; Fan, X.; Gou, L.; Wang, J.; Li, Y.; Lu, X.; Li, Q. Facile Synthesis of Sn−C Nanocomposite as an Anode Material for Lithium Ion Batteries. *J. Alloys Compd.* **2012**, *516*, 33−37.
(19) Zhao, K.; Liu, F.; Niu, C.; Xu, W.; Dong, Y.; Zhang, L.; Xie, S.; Yan, M.; Wei, Q.; Zhao, D.; Mai, L. Graphene Oxide Wrapped Amorphous Copper Vanadium Oxide with Enhanced Capacitive Behavior for High-Rate and Long-Life Lithium-Ion Battery Anodes. *Adv. Sci.* **2015**, *2* (12), 1500154.
(20) Mueller, F.; Bresser, D.; Chakravadhanula, V. S. K.; Passerini, S. Fe-doped SnO_2 Nanoparticles as New High Capacity Anode Material for Secondary Lithium-ion Batteries. *J. Power Sources* **2015**, *299*, 398−402.
(21) Zhang, L.; Zhao, K.; Xu, W.; Dong, Y.; Xia, R.; Liu, F.; He, L.; Wei, Q.; Yan, M.; Mai, L. Integrated SnO_2 Nanorod Array With Polypyrrole Coverage for High-Rate and Long-Life Lithium Batteries. *Phys. Chem. Chem. Phys.* **2015**, *17*, 7619−7623.

DOI: 10.1021/acsami.6b03383
ACS Appl. Mater. Interfaces XXXX, XXX, XXX−XXX

(22) Liu, N.; Wu, H.; McDowell, M. T.; Yao, Y.; Wang, C.; Cui, Y. A Yolk-Shell Design for Stabilized and Scalable Li-ion Battery Alloy Anodes. *Nano Lett.* **2012**, *12* (6), 3315−3321.
(23) Wu, H.; Chan, G.; Choi, J. W.; Ryu, I.; Yao, Y.; McDowell, M. T.; Lee, S. W.; Jackson, A.; Yang, Y.; Hu, L.; Cui, Y. Stable Cycling of Double-Walled Silicon Nanotube Battery Anodes Through Solid−Electrolyte Interphase Control. *Nat. Nanotechnol.* **2012**, *7* (5), 310−315.
(24) Hu, J.; Zheng, J.; Tian, L.; Duan, Y.; Lin, L.; Cui, S.; Peng, H.; Liu, T.; Guo, H.; Wang, X.; Pan, F. A Core-Shell Nanohollow-γ-Fe2O3@Graphene Hybrid Prepared through the Kirkendall Process as High Performance Anode Materials for Lithium Ion Battery. *Chem. Commun.* **2015**, *51* (37), 7855−7858.
(25) Ke, F.-S.; Huang, L.; Cai, J.-S.; Sun, S.-G. Electroplating Synthesis and Electrochemical Properties of Macroporous Sn−Cu Alloy Electrode for Lithium-ion Batteries. *Electrochim. Acta* **2007**, *52* (24), 6741−6747.
(26) Lo Faro, M.; Frontera, P.; Antonucci, P.; Aricò, A. S. Ni−Cu Based Catalysts Prepared by Two Different Methods and Their Catalytic Activity toward the ATR of Methane. *Chem. Eng. Res. Des.* **2015**, *93*, 269−277.
(27) Wu, Y.; Chou, H.; Ji, H.; Wu, Q.; Chen, S.; Jiang, W.; Hao, Y.; Kang, J.; Ren, Y.; Piner, R. D.; Ruoff, R. S. Growth Mechanism and Controlled Synthesis of AB-Stacked Bilayer Graphene on Cu-Ni Alloy Foils. *ACS Nano* **2012**, *6* (9), 7731−7738.
(28) Li, J.-T.; Swiatowska, J.; Seyeux, A.; Huang, L.; Maurice, V.; Sun, S.-G.; Marcus, P. XPS and ToF-SIMS Study of Sn−Co Alloy Thin Films as Anode for Lithium Ion Battery. *J. Power Sources* **2010**, *195* (24), 8251−8257.
(29) Grosvenor, A. P.; Biesinger, M. C.; Smart, R. S. C.; McIntyre, N. S. New Interpretations of XPS Spectra of Nickel Metal and Oxides. *Surf. Sci.* **2006**, *600* (9), 1771−1779.
(30) Espinós, J. P.; Morales, J.; Barranco, A.; Caballero, A.; Holgado, J. P.; González-Elipe, A. R. Interface Effects for Cu, CuO, and Cu_2O Deposited on SiO_2 and ZrO_2. XPS Determination of the Valence State of Copper in Cu/SiO_2 and Cu/ZrO_2 Catalysts. *J. Phys. Chem. B* **2002**, *106*, 6921−6929.
(31) Ferrari, A. C.; Meyer, J. C.; Scardaci, V.; Casiraghi, C.; Lazzeri, M.; Mauri, F.; Piscanec, S.; Jiang, D.; Novoselov, K. S.; Roth, S.; Geim, A. K. Raman Spectrum of Graphene and Graphene Layers. *Phys. Rev. Lett.* **2006**, *97* (18), 187401.
(32) Díaz, J.; Paolicelli, G.; Ferrer, S.; Comin, F. Separation of the sp^3 and sp^2 Components in the C1s Photoemission Spectra of Amorphous Carbon Film. *Phys. Rev. B: Condens. Matter Mater. Phys.* **1996**, *54* (11), 8064−8069.
(33) Li, X.; Cai, W.; Colombo, L.; Ruoff, R. S. Evolution of Graphene Growth on Ni and Cu by Carbon Isotope Labeling. *Nano Lett.* **2009**, *9* (12), 4268−4272.
(34) Guo, Z. P.; Zhao, Z. W.; Liu, H. K.; Dou, S. X. Electrochemical Lithiation and De-lithiation of MWNT−Sn/SnNi Nanocomposites. *Carbon* **2005**, *43* (7), 1392−1399.
(35) Hassoun, J.; Derrien, G.; Panero, S.; Scrosati, B. A Nano-structured Sn-C Composite Lithium Battery Electrode with Unique Stability and High Electrochemical Performance. *Adv. Mater.* **2008**, *20* (16), 3169−3175.
(36) Xu, Y.; Liu, Q.; Zhu, Y.; Liu, Y.; Langrock, A.; Zachariah, M. R.; Wang, C. Uniform Nano-Sn/C Composite Anodes for Lithium Ion Batteries. *Nano Lett.* **2013**, *13* (2), 470−474.
(37) Sun, L.; Wang, X.; Susantyoko, R. A.; Zhang, Q. High Performance Binder-Free Sn Coated Carbon Nanotube Array Anode. *Carbon* **2015**, *82*, 282−287.
(38) Xu, K. Nonaqueous Liquid Electrolytes for Lithium-Based Rechargeable Batteries. *Chem. Rev.* **2004**, *104*, 4303−4417.

DOI: 10.1021/acsami.6b03383
ACS Appl. Mater. Interfaces XXXX, XXX, XXX−XXX